J. Fluid Mech. (1976), *vol.* 77, *part* 4, *pp.* 645–664
Printed in Great Britain

Wind-induced turbulent heat and mass transfer over large bodies of water

By C. Y. SHAW† AND Y. LEE
Department of Mechanical Engineering, University of Ottawa, Canada K1N 6N5

(Received 23 February 1976)

A semi-theoretical study has been made of the problem of stable turbulent heat and mass transfer between a water surface and surrounding atmosphere under the influence of wind. The equations derived are based on the principle of similarity and are therefore expected to be valid under both laboratory and field conditions. The predicted heat- and mass-transfer Stanton numbers appear to be in satisfactory agreement with the available field data.

1. Introduction

The problem of turbulent heat and mass transfer at an air–water interface has been extensively studied, but the conclusions of the various investigators have been in poor agreement with one another (e.g. Braslavskii & Vikulina 1963; Mangarella *et al.* 1973; Marciano & Harbeck 1954). With a few exceptions (Calder 1949; Shaw & Lee 1974), previous correlations have been deduced mainly from experimental data. These data involve the temperature and specific-humidity distributions above a wavy water surface. In the region close to the interface, where the profiles undergo a sharp change, these distributions cannot be measured accurately because of the presence of waves and spray. Therefore, when these data are extrapolated down to the water surface in order to evaluate the heat- or mass-transfer Stanton number, serious error may result.

This study attempts to solve the problem semi-analytically. The calculation is based on the two-dimensional boundary-layer equations of momentum, energy and diffusion. The effect of fetch (distance between measuring station and shore) on various flow parameters, such as shear velocity and dynamic roughness, are included in the dimensionless form of these equations. An experimental study has also been conducted, using an environmentally controlled wind–water tunnel. The analytical solution and the measurements are compared to check the validity of the theory under the conditions specified.

2. Analysis

Basic equations

For steady two-dimensional turbulent flow of an incompressible fluid with negligible dissipation, the boundary-layer equations of energy, diffusion and

† Present address: Division of Building Research, National Research Council of Canada, Ottawa, Canada.

continuity are

$$u\frac{\partial t}{\partial x}+v\frac{\partial t}{\partial y}=\frac{\partial}{\partial y}\left|(\alpha+\epsilon_H)\frac{\partial t}{\partial y}\right|, \tag{1}$$

$$u\frac{\partial m}{\partial x}+v\frac{\partial m}{\partial y}=\frac{\partial}{\partial y}\left|(\beta+\epsilon_D)\frac{\partial m}{\partial y}\right| \tag{2}$$

and

$$\partial u/\partial x+\partial v/\partial y=0 \tag{3}$$

respectively, where x and y are the streamwise and transverse co-ordinates, u and v are the x and y components of the wind velocity, t and m are the temperature and specific humidity, α and β are the thermal diffusivity and diffusion coefficient and ϵ_H and ϵ_D are eddy diffusivities of heat and mass. Equations (1) and (3) can be made dimensionless by substituting the dimensionless parameters derived in the appendix:

$$-0{\cdot}82u^+\frac{\partial\tilde{F}}{\partial x^{++}}+\left(v^+ +\frac{0{\cdot}19k}{\epsilon_e}\right)\frac{\partial\tilde{F}}{\partial y^{++}}=\frac{k}{\epsilon_e}\frac{\partial}{\partial y^{++}}\left(y^{++}\frac{\partial\tilde{F}}{\partial y^{++}}\right), \tag{4}$$

$$\frac{\partial v^+}{\partial y^{++}}=\frac{1{\cdot}82}{kx^{++}}-0{\cdot}34\frac{u^+}{x^{++}}+0{\cdot}19\frac{v^+}{y^{++}}. \tag{5}$$

Equation (4) can be solved using a finite-difference method of the Dufort–Frankel type (Pletcher 1969). The boundary and initial conditions are

$$\begin{aligned}
&u^+=0,\quad v^+=0,\quad \tilde{F}=0 \quad \text{on} \quad y^{++}=1,\\
&u^+=u_r^+,\quad \tilde{F}=1 \quad \text{as} \quad y^{++}\to\infty,\\
&\tilde{F}=0 \quad \text{on} \quad x^{++}=0,\quad y^{++}=1,\\
&\tilde{F}=1 \quad \text{on} \quad x^{++}=0,\quad y^{++}>1.
\end{aligned}$$

The appropriate grid size was selected by estimating a suitable height y_1^{++} of the nodal point immediately above the water surface. This was done by assuming various values for y_1^{++} and comparing the corresponding values of $\tilde{F}$. It was found that there is no significant dependence of $\tilde{F}$ on y_1^{++} if y_1^{++} is between 10 and 20. Thus the values of y_1^{++} selected was 10. The values of Δx^{++} chosen was ~ 20.

Heat- and mass-transfer Stanton numbers

The heat and mass fluxes at any point within a fluid are given by

$$q=-\rho C_p\nu\left(\frac{1}{Pr}+\frac{\epsilon_H}{\nu}\right)\frac{dt}{dy}, \tag{6}$$

$$e=-\rho\nu\left(\frac{1}{Sc}+\frac{\epsilon_D}{\nu}\right)\frac{dm}{dy}, \tag{7}$$

where q and e are the heat and mass transfer rates, Pr ($=\nu/\alpha$) and Sc ($=\nu/\beta$) are the Prandtl and Schmidt numbers and ν, ρ and C_p are the kinematic viscosity, density and specific heat at constant pressure, respectively.

In dimensionless form (6) and (7) can be written as

$$G=(\epsilon_v+\epsilon_c)\,d\tilde{F}/dy^{++}, \tag{8}$$

where ϵ_v is Pr^{-1} for heat transfer and Sc^{-1} for mass transfer and

$$G = \begin{cases} qz_0/\rho c_p(t_{z_0}-t_r)\,\nu & \text{for heat transfer,} \\ ez_0/\rho(m_{z_0}-m_r)\,\nu & \text{for mass transfer.} \end{cases}$$

If we let $\epsilon_c = e_M/\nu$, we can obtain the following from equation (A 11) of the appendix:

$$\frac{e_M}{\nu} = \frac{kz_0(\tau_0/\rho)^{\frac{1}{2}}\,y^{++}}{\nu} - 1.$$

Then (8) can be rewritten as

$$G = \left(\frac{kz_0(\tau_0/\rho)^{\frac{1}{2}}\,y^{++}}{\nu} + \epsilon_v - 1\right)\frac{d\tilde{F}}{dy^{++}}. \tag{9}$$

The heat-transfer and mass-transfer Stanton numbers are defined by

$$St_H = \frac{q}{\rho c_p\,u_r(t_{z_0}-t)} \quad \text{for heat transfer,} \tag{10}$$

$$St_D = \frac{e}{\rho u_r(m_{z_0}-m)} \quad \text{for mass transfer.} \tag{11}$$

The subscripts r and z_0 refer to the conditions at a reference height above the mean water level and at the height of dynamic roughness $y = z_0$, respectively.

Integrating (9) from $y^{++} = 1$ to y^{++} and then combining the resultant expression with (10) or (11) to eliminate q or e, we have

$$St_D \text{ or } St_H = k^2\left\{\ln y_r^{++}\ln\left|\frac{kz_0u_r\nu^{-1}y_r^{++}+\epsilon_v-1}{kz_0u_r\nu^{-1}+\epsilon_v-1}\right|\right\}^{-1}. \tag{12}$$

Since, as shown in the appendix, z_0 is a function of Froude numbers defined by $Fr_{Ly} = u/(gL^{0\cdot8}y^{0\cdot2})^{\frac{1}{2}}$ and $Fr_y = u/(gy)^{\frac{1}{2}}$, the Stanton number is also a function of these two quantities. Here L is the fetch and y is vertical distance.

3. Experiment

Air–water tunnel

All measurements were made in the closed-circuit air–water tunnel shown in figure 1. Briefly, it consists of five parts: a fan section, an entrance with a straight duct 853 cm long, a working section 351 cm in length, a return duct and an environmental control system.

The fan section consists of an air filter chamber, a cooling coil, an electric heating coil and two centrifugal fans, enclosed in a common steel cabinet. The total capacity of the fans is 3·6 m^3/s at a static pressure difference of 622 N/m^2. The maximum attainable wind speed in the tunnel is about 20 m/s. The fans are equipped with a common Torq-matic solid-state variable-speed drive. With this variable-speed drive, the fan can be controlled at any speed up to 1800 r.p.m. with an accuracy of $\pm 1\%$.

The working section consists of an air passage 47·5 cm wide by 30·4 cm high and a water reservoir of the same dimensions. A beach which makes an angle of about 5° with the water surface is installed at the leading edge of the reservoir.

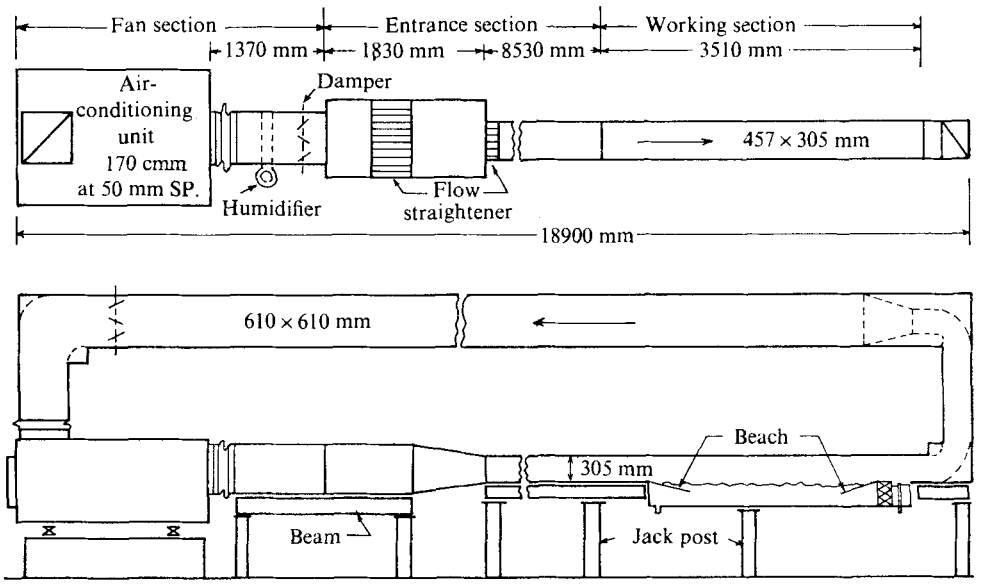

FIGURE 1. Air–water tunnel.

This angle has been chosen by trial and error. This angle should be small enough to ensure a smooth transition between the adjoining air and water flows but should not be too small to affect the normal growth of the wave.

The top of the working section consists of five pieces with lengths varying from 30·5 cm to 91·4 cm. All the measuring probes except the thermocouple for measuring the temperature at the mean water level are attached to one of the top pieces 45·7 cm long. The top pieces are interchangeable, so that the measuring probe can be located at various positions along the working section by placing various combinations of the top pieces ahead of it. To minimize air leakage through the gap between two adjacent pieces, various lengths of polished stainless-steel plate are provided so that one of these plates can be fitted underneath the top pieces. The measuring probes can also be placed at any lateral position within 20·3 cm away from the centre by sliding the probes in a slot cut in the top piece. The portion of the slot that is not occupied by the probes is filled with small pieces of well-machined wood blocks to reduce air leakage.

This tunnel differs from those used by most other investigators (e.g. Mangarella *et al.* 1973) in the following respects.

(i) It has a long entrance duct: this is necessary to ensure fully developed flow, hence eliminating hydrodynamic entrance effects at the test station.

(ii) It has an environmental control system. This system has a 10·6 kW refrigeration plant and a steam humidifier. It provides a close control on the temperature as well as the humidity at the entrance of the working section. The accuracy of the controllers is 1% of the full span.

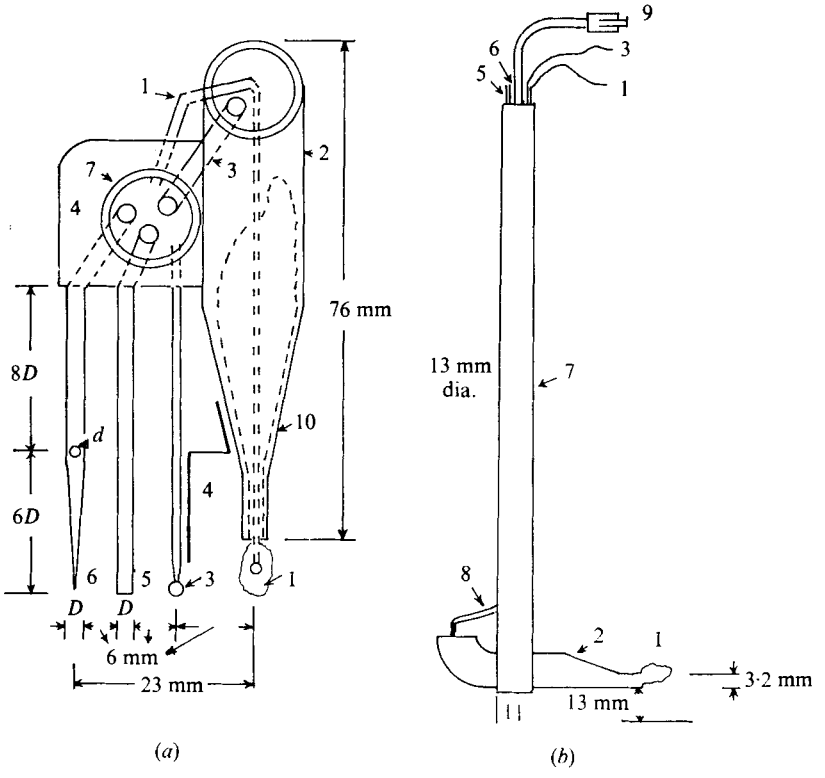

FIGURE 2. Measuring probe. (*a*) Plan. (*b*) Elevation. D = 1·1 mm, d = 0·25 mm. 1, wet-bulb thermocouple; 2, water reservoir; 3, support; 4, total-pressure tube; 5, dry-bulb thermocouple; 6, static-pressure tube; 7, traverse tube; 8, make-up water supply; 9, syringe; 10, cotton; 11, needle.

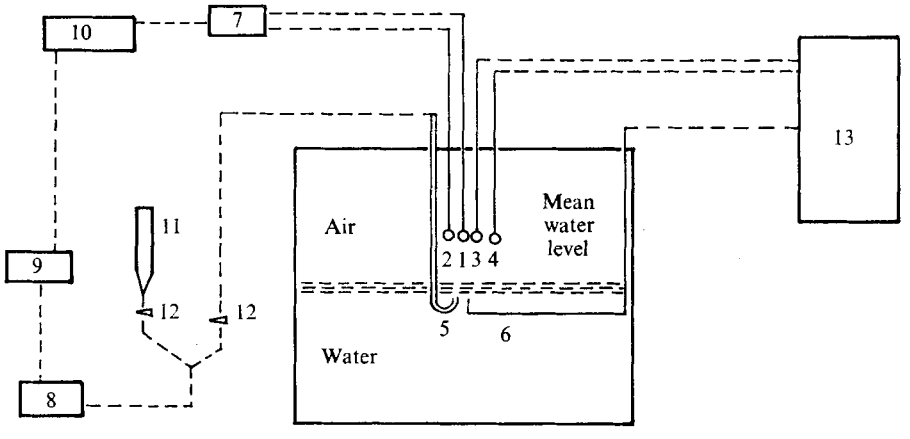

FIGURE 3. Schematic diagram of measuring system. 1, total-pressure tube; 2, static-pressure tube; 3, dry-bulb thermocouple; 4, wet-bulb thermocouple; 5, wave probe; 6, thermocouple; 7, Statham strain-gauge differential pressure transducer; 8, Endevco strain-gauge differential pressure transducer; 9, DISA 55D35 r.m.s. voltmeter; 10, Hewlett–Packard HP4100B two-channel strip-chart recorder; 11, burette for wave-probe calibration; 12, shut-off valve; 13, Hewlett–Packard 2010K data acquisition system.

Measuring instruments and procedure

(i) *Multiple-function measuring probe.* As shown in figure 2, a multiple-function measuring probe about 2·3 cm wide by 0·32 cm high has been developed for measuring the velocity as well as dry- and wet-bulb temperature profiles. The probe is composed of a static-pressure tube, a total-pressure tube, a dry-bulb thermocouple, a wet-bulb thermocouple and a water reservoir for the wet-bulb thermocouple. A dial height gauge is attached to the probe for evaluating the vertical distance above the mean water level.

(ii) *Wave gauge.* The wave gauge shown in figure 3 was developed for the measurement of the wave amplitude. It is made of a copper tube of outside diameter 0·64 cm. One end of the tube is bent to form a U so that when it is submerged in water its tip is normal to the mean water level. Measurement of the wave height with this instrument seems to be simpler than measurement based on electrical resistance and capacitance. A burette is connected to the wave-amplitude circuit upstream of the pressure transducer for calibration. Two valves are installed in the circuit so that the pressure transducer can be switched to measure the water level of either component during the test.

(iii) *Evaluation of the shear velocity, dynamic roughness, drag coefficient, temperature and specific humidity.* The shear velocity and the dynamic roughness are evaluated by fitting the velocity data to the velocity profile given by

$$\frac{u}{u_\tau} = \frac{1}{k}\ln\left(\frac{y}{z_0}\right). \tag{13}$$

This equation will be discussed in the appendix. Using the shear velocity, the drag coefficient can then be calculated from the definition

$$C_i = 2(u_\tau/u_i)^2. \tag{14}$$

The specific humidity is evaluated from a psychrometric table using the measured dry- and wet-bulb temperatures.

4. Results and discussion

Velocity profile

Since the probe was never closer than $5a_{\text{r.m.s.}}$ to the mean water level, the error induced by the moving boundary should be negligible (Chambers *et al.* 1970).

A selection of typical mean velocity profiles is shown in figure 4. It may be seen that the experimental data can be represented quite well by the equation

$$\frac{u}{u_\tau} = \frac{1}{k}\ln\frac{y}{z_0}. \tag{15}$$

In this study, about 10% of the measured profiles deviate slightly from the logarithmic profile. Of this 10%, except at those stations that are near the mean water level and the centre-line of the tunnel, these deviations are less than 3%. Further examination of this 10% of the measured velocity profiles indicates that these measurements were conducted at large fetch under the condition of

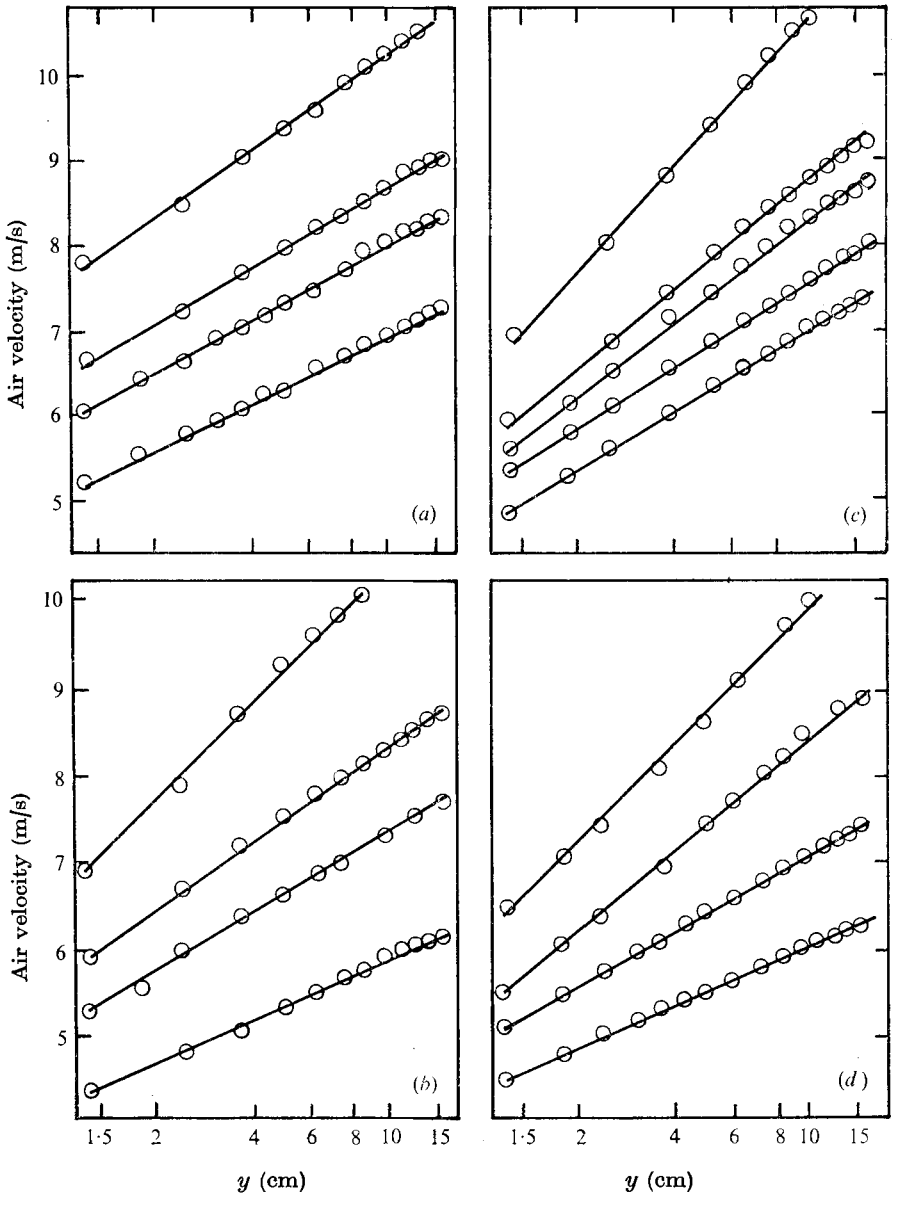

FIGURE 4. Air velocity distribution. (*a*) L = 380 mm. (*b*) L = 970 mm. (*c*) L = 1300 mm. (*d*) L = 1980 mm.

high centre-line air velocity. Since the presence of spray is usually observed at large fetch and high centre-line air velocity, the poor agreement between the measured data and the logarithmic law near the mean water level may have been caused by partial blockage of the static-pressure probe by spray.

The air–water temperature difference does not appear to affect the mean air velocity profile for centre-line velocities ranging from 3 to 25 m/s and an air–

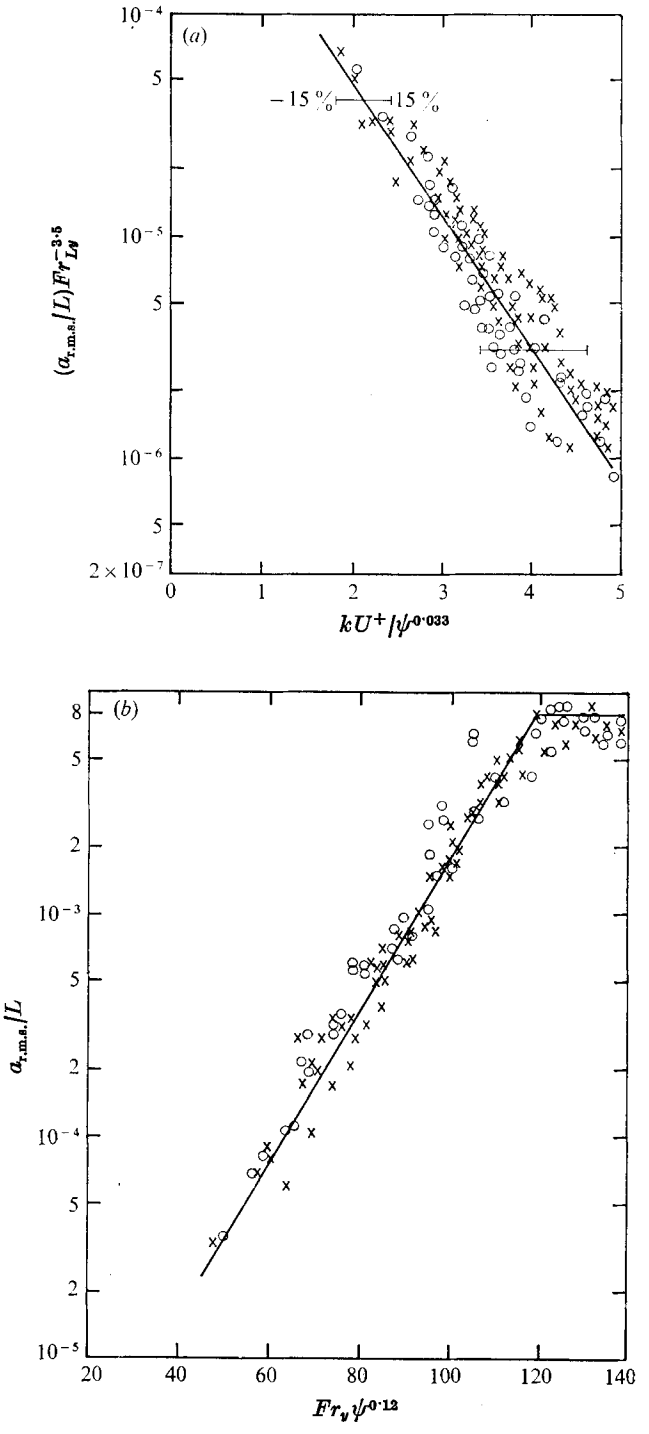

FIGURE 5. (*a*) Relationship among $a_{r.m.s.}/L$, the Froude number and u^+. (*b*) Relationship between $a_{r.m.s.}/L$ and Fr_y. ×, $\psi = 150\times10^5$; ○, $\psi = 18\times10^5$. $\psi \equiv (uy/\nu)^2(u^2/gy)^{-1}$.

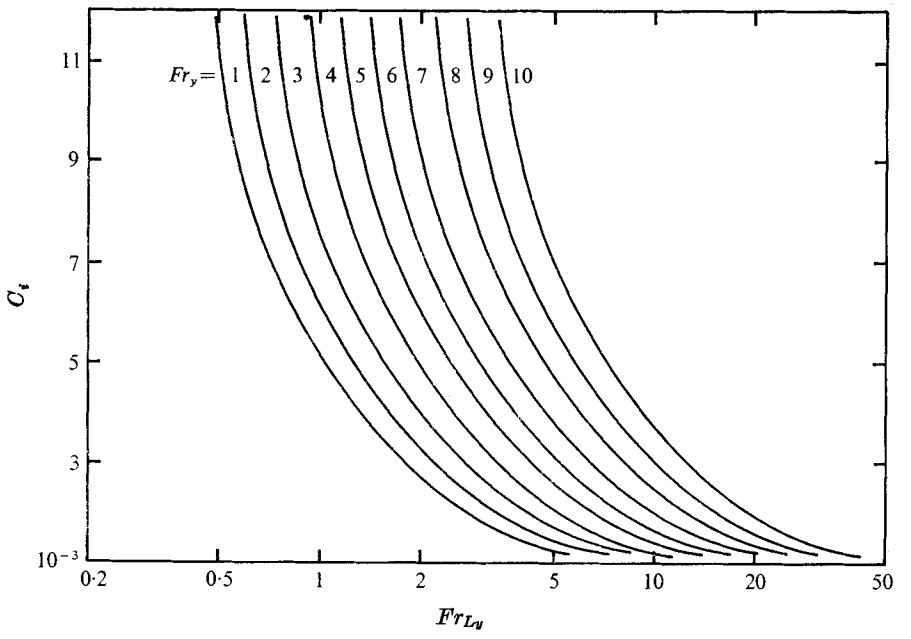

FIGURE 6. Wind-induced drag coefficient.

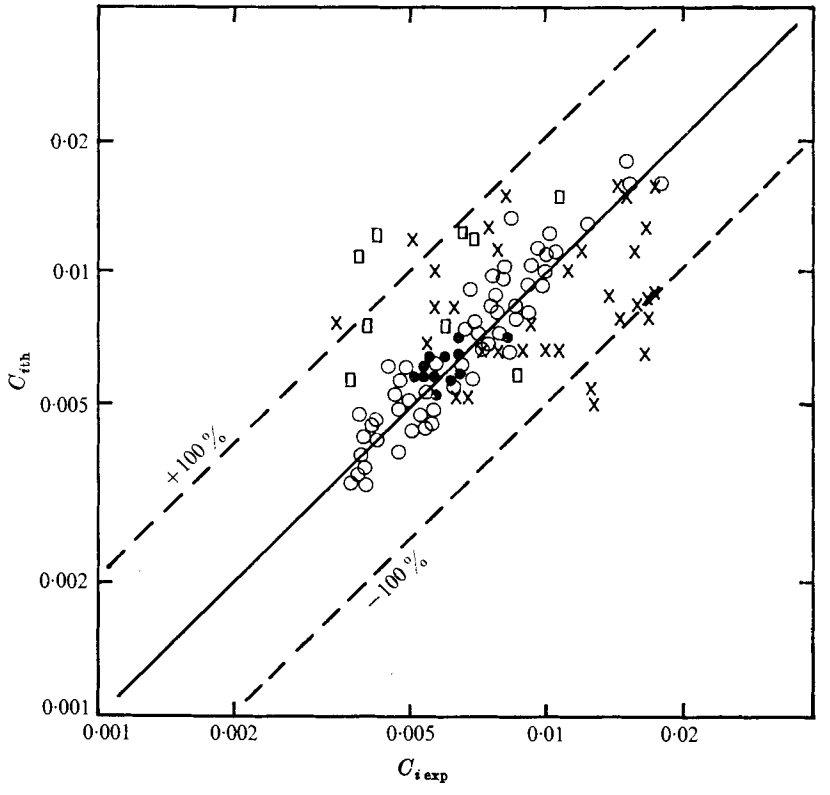

FIGURE 7. Comparison of predicted and experimental drag coefficients. ○, present study; ●, Gottifredi & Jameson; ×, Chambers *et al.*; □, Hidy & Plate.

water temperature difference up to 21 °C. This conclusion was also reported by Chambers *et al.* (1970). The values of the Richardson number

$$Ri = \left(\frac{g}{t}\frac{dt}{dy}\right) \Big/ \left(\frac{du}{dy}\right)^2$$

at 10 cm were less than 5×10^{-4}, which indicates that the influence of thermal stratification is also negligible.

The functional relationships among $a_{\text{r.m.s.}}/L$, Fr_{Ly} and u^+ and between $a_{\text{r.m.t.}}/L$ and Fr_y are given by (A 7) and (A 8) respectively. These relationships were obtained by fitting the experimental data of the present study with curves derived on the basis of dimensional analysis. As shown in figures 5(*a*) and (*b*), the average deviations between the experimental data and the curves defined by (A 7) and (A 8) are about 15% and 50% relative to the equations.

The drag coefficient predicted by (A 9) is shown in figure 6. The predicted and measured values of the drag coefficient are compared in figure 7. The agreement is fair. The calculated drag coefficient is also compared with the experimental data obtained by Gottifredi & Jameson (1970), Chambers *et al.* (1970) and Hidy & Plate (1966) in figure 7. To be consistent our results were calculated using the same velocities and vertical distances as were used by these investigators. Where the average velocity was used it was multiplied by 1·25 to convert it back to the reference velocity as it was by Hidy & Plate (1966). The work of Gottifredi & Jameson (1970) is very interesting in view of the method used for estimating the drag coefficient. The shear velocity was calculated by fitting the experimental data to the velocity profile

$$u^+ = y^+, \quad 0 < y < y_1.$$

Here y_1 is the thickness of the laminar sublayer, which exists only if the wave is totally submerged within the layer. This method is superior to the profile method in that u can be calculated uniquely. The reliability of the method depends upon the accuracy of the velocity measurements within the laminar sublayer, which, in turn, is governed by the wave height. In general, if the air velocities are measured at small fetch under the condition of low wind, the accuracy of the u_τ calculated from these measurements should be highly dependable. On the basis of the above consideration, the result obtained by Gottifredi & Jameson at small fetch (46 cm) and low air velocity ($u_\tau \leqslant 3{\cdot}15$ m/s) was selected as the base for checking the validity of the analytical solution. As shown in the figure, the agreement is extremely good. The experimental data deduced using the profile method spread quite evenly on both sides of the 45° line. Unlike the equipment used by the author or by Gottifredi & Jameson (1970), the air–water tunnels used by Chambers *et al.* (1970) and Hidy & Plate (1966) did not have a long entrance section prior to the water tank. Since the drag coefficient is strongly affected by the velocity profile, the lack of an entrance section may affect the results. The difference in the flow conditions is believed to be partially responsible for the wide gap between the analytical and measured drag coefficients.

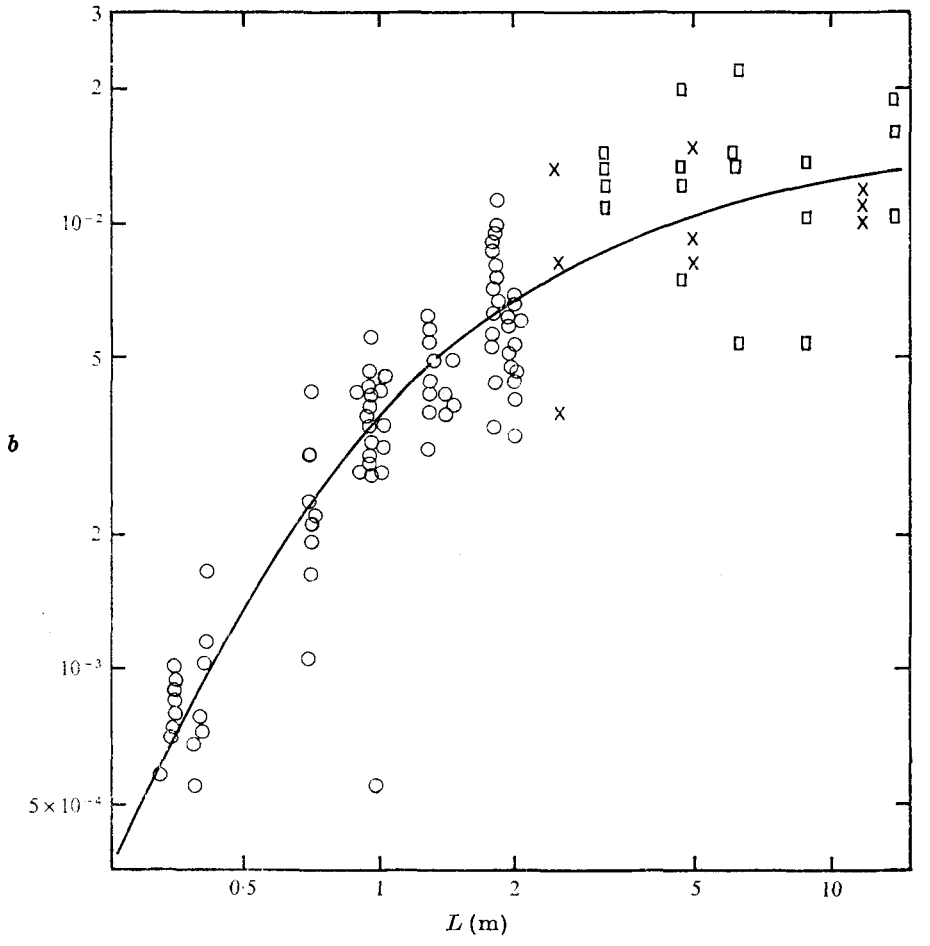

FIGURE 8. Charnock's constant. Symbols as in figure 7.

Charnock (1955) suggested that the following expression links the dynamic roughness to the shear velocity:

$$b = z_0 g/u_\tau^2. \tag{16}$$

On the basis of a large collection of wind-profile measurements obtained in the laboratory as well as over the ocean, Wu (1969) suggested values of 0·0112 and 0·0156 for b for laboratory and ocean conditions respectively. To check the validity of this relationship, values of b deduced from the present study are shown in figure 8. For comparison the values of b obtained by Chambers *et al.* (1970) and Hidy & Plate (1966) are also shown in the figure. The results indicate that b is not constant but a function of fetch. Consequently, (16) can considerably overestimate the value of z_0 and hence C_i at small fetch if b is assumed constant as suggested by Wu (1969).

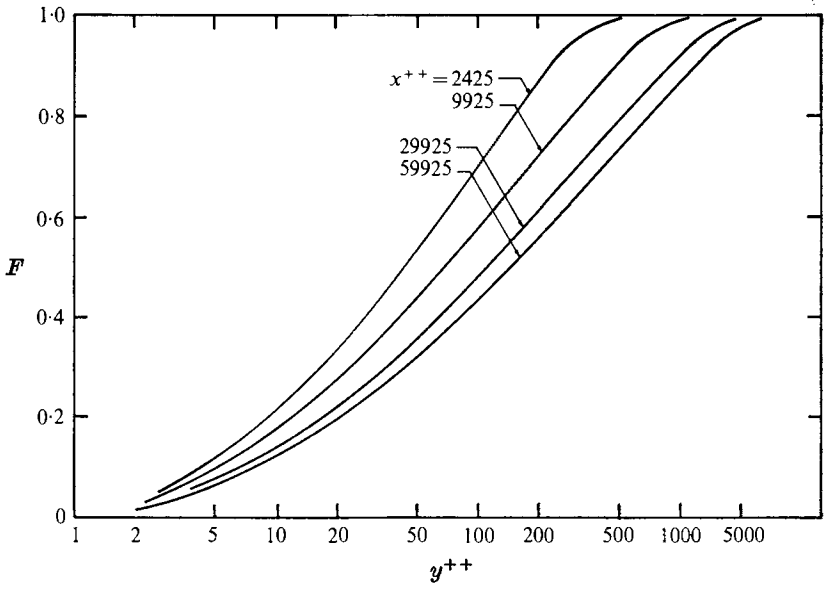

FIGURE 9. Dimensionless temperature and specific-humidity profiles.

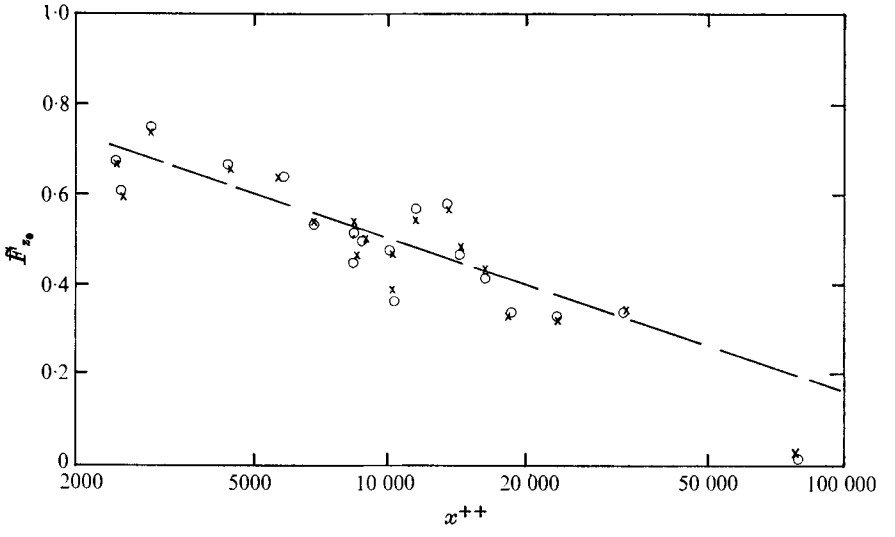

FIGURE 10. Temperature (crosses) and specific humidity (circles) at $y^{++} = 1$. $F_{z_0} = (t_0 - t_{z_0})/(t_0 - t_r)$ or $(m_0 - m_{z_0})/(m_0 - m_r)$.

Temperature and specific-humidity profiles

The calculated temperature and specific-humidity distributions are shown in figure 9. It is evident that these profiles are functions of both x^{++} and y^{++}. The dependence on x^{++} becomes less pronounced as x^{++} increases.

These profiles were normalized using the temperature and the specific humidity at the distance z_0 above the mean water level. The relationship between these values and those at the mean water level is shown in figure 10. It is evident that

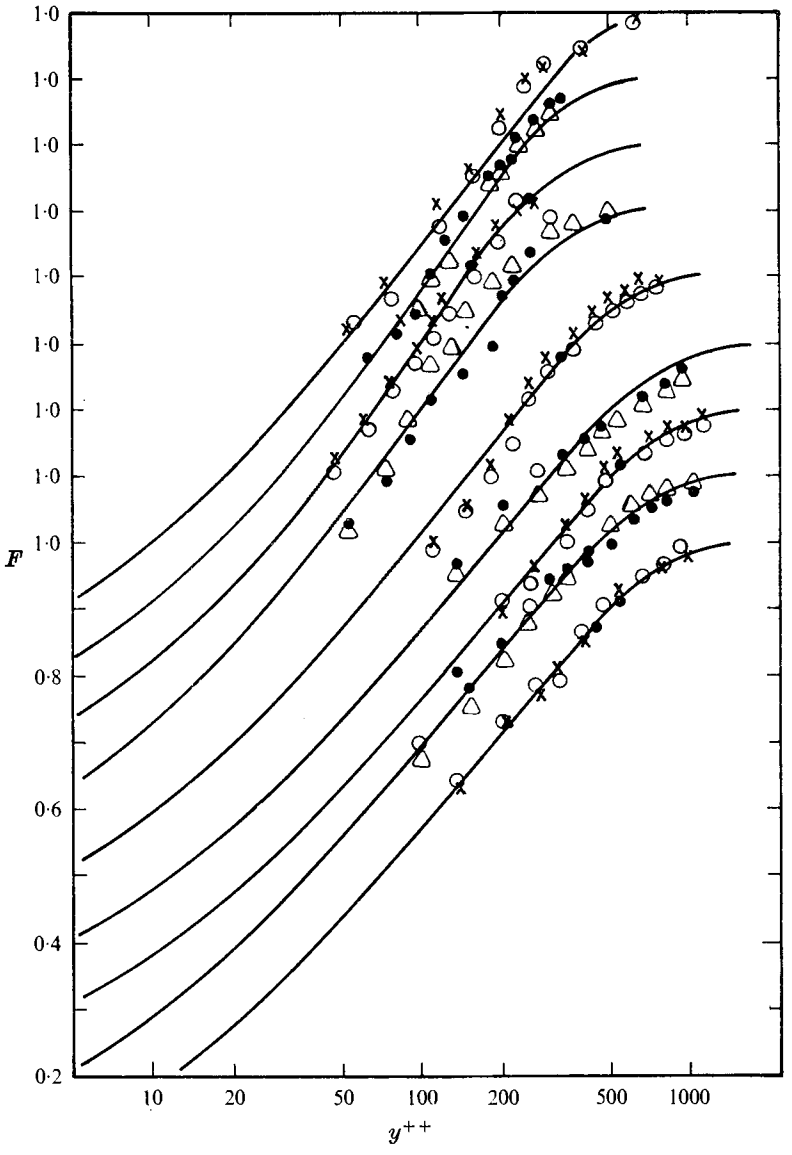

FIGURE 11. Comparison of values of the parameter F. —, present theory. Experiment: ×, △, temperature; ○, ●, specific humidity. Note shifted vertical co-ordinate.

the differences in temperature as well as in specific humidity between these two levels are higher at smaller values of x^{++} than at larger x^{++}. This seems to imply that at very large fetch ($dx^{++}/dx \to$ constant) the temperature and specific humidity at $y = z_0$ both approach their values at the mean water level.

The calculated and measured profiles are compared in figure 11. Good agreement is achieved. It is also shown in this figure that the normalized temperature and specific-humidity profiles coincide with each other. This result supports the assumption of a turbulent Lewis number of unity.

There is a fundamental difference in the normalization of the temperature and the specific-humidity profiles used here and by other investigators (Mangarella *et al.* 1972, 1973). In the present study, the temperature and specific humidity at $y = z_0$ were used instead of the values at the water surface.

The choice of reference point discussed above may have a significant effect in the evaluation of the transfer coefficients. These coefficients can be calculated either by evaluating the first derivative of the profile at the reference point or by estimating the enthalpy thickness for the case of heat transfer and its counterpart for the case of mass transfer. In either case, a complete description of the temperature or the specific-humidity profiles, especially in the region where these profiles undergo a sharp change, is essential. If the reference point is chosen to be the mean water level, the transfer coefficients cannot be accurately determined because the temperature and specific-humidity distributions in the region between $y = 0$ and $y = z_0$ are not known. Moreover, the distribution of air velocity in this region is also unknown. On the other hand, if the reference point is chosen at the height z_0 above the mean water level, where the air velocity is assumed to be zero, all the profiles from this level upwards through the boundary layer are fully described and the transfer coefficients based on this reference point can be calculated.

Heat- and mass-transfer Stanton numbers

The heat- and mass-transfer Stanton numbers based on (12) are shown in figure 12. They are functions of both Fr_y and Fr_{Ly}. Since these two Froude numbers are closely related to u_τ and z_0, the Stanton numbers may also be expressed in terms of the roughness Reynolds number ($Re_{z_0} = u_\tau z_0/\nu$). Accordingly, the predicted heat- and mass-transfer Stanton numbers were evaluated using different Prandtl numbers and Schmidt numbers. The Stanton numbers based on $Pr = 0{\cdot}72$ and $Sc = 0{\cdot}6$ are shown in figure 13(*a*) whereas those based on $Pr = Sc = 1$ are shown in figure 13(*b*). As shown in these two figures, the Stanton number is a function of both the roughness Reynolds number ($u_\tau z_0/\nu$) and the Froude number $[u_r/(gy_r)^{\frac{1}{2}}]$. These figures also show that the Stanton number based on $Pr = Sc = 1$ can be as much as 30% lower than that based on $Pr = 0{\cdot}72$ and $Sc = 0{\cdot}6$. Although the Prandtl and Schmidt numbers both vary with air temperature, their numerical values are approximately equal to 0·72 and 0·6, respectively, for the temperature range under consideration. The Stanton numbers based on $Pr = Sc = 1$ are shown here so that they can be compared with the field data compiled by Kitaigorodskii & Volkov (1965) from the profile measurements of other investigators (Takahashi 1958; Snopkof 1965; Deardorff 1962; Fleagle, Deardorff & Badgley 1958) under the assumption that the Prandtl and Schmidt numbers are unity.

For $Pr = Sc = 1$, (12) simplifies to

$$St_D = St_H = k^2 (\ln y_r^{++})^2. \tag{17}$$

Since the Stanton number is a function of y_r^{++}, the right-hand side of (17) can

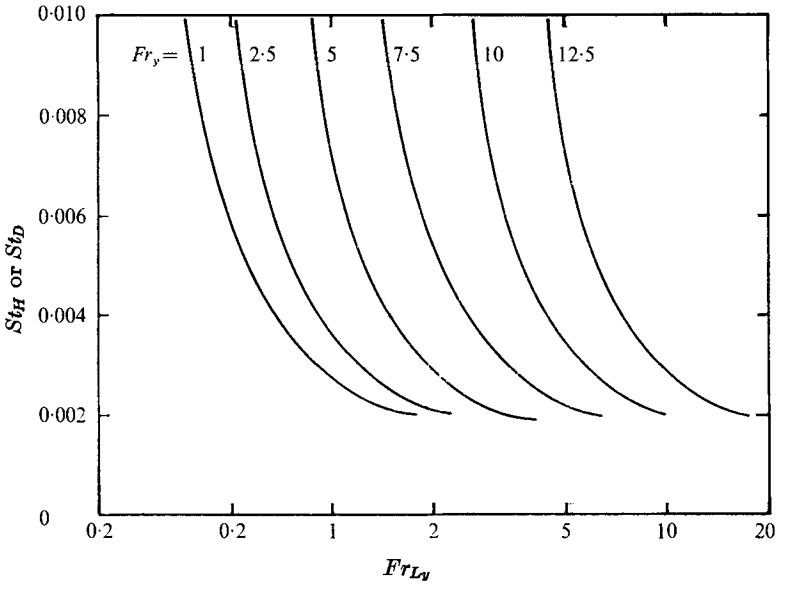

FIGURE 12. Stanton numbers.

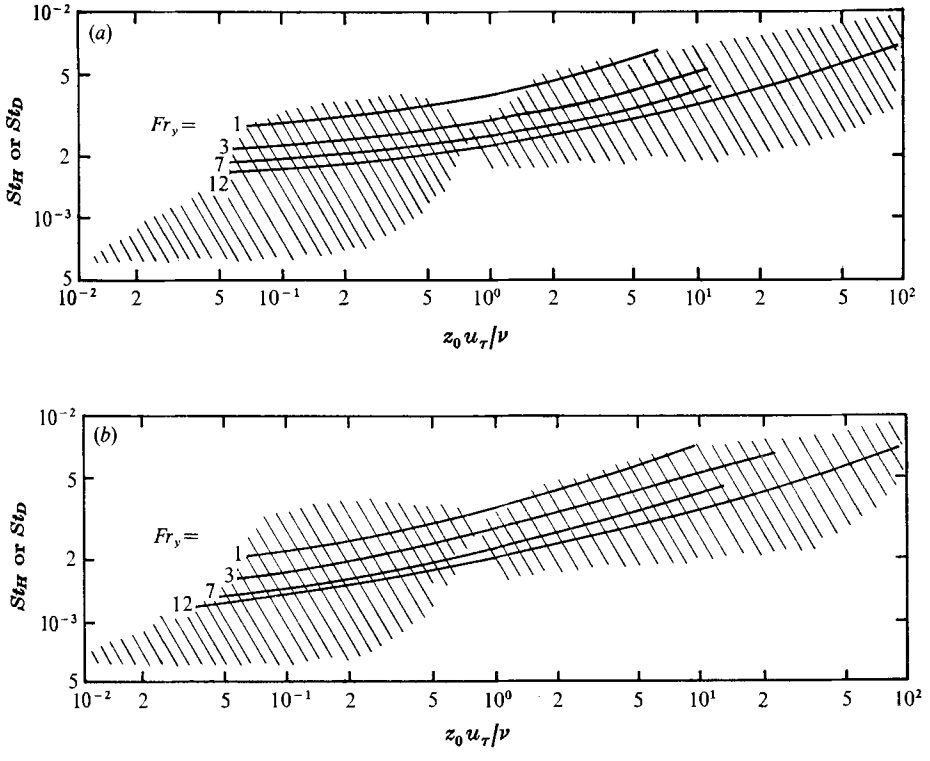

FIGURE 13. Comparison of predicted Stanton numbers and field data. (*a*) $Pr = 0{\cdot}7$, $Sc = 0{\cdot}6$. (*b*) $Pr = Sc = 1$. ——, present theory; ▨, field data based on work of four investigators.

be expressed in terms of u and z_0. Introducing the roughness Reynolds number the following relationship may be established:

$$St_D \doteq St_H \doteq \phi_2(Re_{z_0}). \tag{18}$$

Finally, evaluating the Stanton number from (17) and using the method of curve fitting, we have

$$St_D = St_H = 0{\cdot}0035 Fr_y^{-0{\cdot}2}(Re_{z_0})^{0{\cdot}22}. \tag{19}$$

Because the parameter $u_r/(gy_r)^{\frac{1}{2}}$ was not considered as a variable in the evaluation of the field data, a rigorous comparison between the present theory and these field measurements cannot be made. However, it can be seen from figures 13(*a*) and (*b*) that the agreement between the analysis and the field data is quite satisfactory. Figures 13(*a*) and (*b*) show that there is a large scatter in the field data. Apart from the experimental errors, the scatter in the field data may be partially attributed to the fact that Fr_y has not been considered one of the dominant parameters up to now. However, the influence of Fr_y on the Stanton number can be clearly observed from the analytical results as shown in these figures.

Limitations of the solution

In the analysis, the logarithmic velocity profile is assumed to be valid regardless of stability variations. This assumption is substantiated by the extremely small Richardson number obtained under laboratory conditions. Under field conditions, the validity of the assumption is limited to a region immediately above the water surface owing to a decrease in the influence of the thermal stability as the surface is approached (Monin 1972). The thickness of this region varies from a few metres for the case of very strong stability to a very large value for the case of neutral stability according to Monin (1972). On the basis of the extensive velocity measurements conducted by Marciano & Harbeck (1954), this thickness appears to be 8 m. Therefore, the solution is expected to be valid under field conditions also as long as the flow parameters are evaluated within 8 m from the water surface.

5. Conclusions

(*a*) The mean wind velocity profile can be satisfactorily described by a logarithmic velocity profile. For the temperature range considered, the influence of thermal stability on the velocity profile can be neglected under laboratory conditions. Under field conditions, the logarithmic velocity profile is also valid, regardless of thermal stability, up to approximately 8 m above the mean water level.

(*b*) The agreement between the predicted Stanton numbers and the available field data seems to be quite satisfactory.

(*c*) Further field data are required for the evaluation of Fr_y, Fr_{Ly} and Re_{z_0}.

(*d*) The thermal stability appears to have very little effect on the solution of interfacial heat- and mass-transfer problems since heat and mass transfer are mainly governed by the conditions in the immediate neighbourhood of the water surface, where the influence of thermal stability is negligible.

This research was supported by the Canadian National Research Council and Department of Energy, Mines and Resources of Canada.

Appendix

Velocity distributions

In solving (1) and (3) the mean air velocity profile in the streamwise direction is assumed to be the universal velocity profile for a rough plate (Prandtl 1928):

$$\frac{u}{u_\tau} = \frac{1}{k}\ln\left(\frac{y}{z_0}\right), \tag{A 1}$$

where $u_\tau = (\tau_0/\rho)^{\frac{1}{2}}$ is the shear velocity at the water surface, k is a constant, equal to 0·4, and z_0 is the dynamic roughness. It has been found that (A 1) agrees very well with velocity measurements conducted over oceans (Ruggles 1970), reservoirs (Braslavskii & Vikulina 1963), lakes (Marciano & Harbeck 1954) and wavy surfaces in laboratory air–water tunnels (e.g. Shemdin 1967; Wu 1968; Chambers *et al.* 1960). Measurements have sometimes been made under both adiabatic and diabaric conditions. These results appear to indicate that the effects of changes in thermal stability on the wind velocity profile are negligible in the region close to the water surface.

Functional relationship among variables

For air flow over a wavy water surface, the mean air velocity at a reference height may be expressed as

$$u = \phi(\rho, L, \tau_0, a_{\text{r.m.s.}}, g), \tag{A 2}$$

where $a_{\text{r.m.s.}}$ is the root-mean-square amplitude of the water wave, g is the acceleration due to gravity, L is the fetch, ρ is the density and τ_0 is the shear stress at the water surface. From a dimensional analysis using u, ρ and L as the primary variables we obtain the expression

$$\frac{u}{(\tau_0/\rho)^{\frac{1}{2}}} = \phi_1\left(\frac{a_{\text{r.m.s.}}}{L}, \frac{u}{(gL)^{\frac{1}{2}}}\right). \tag{A 3}$$

From the power-law velocity profile which is often used to approximate the logarithmic velocity profile, we have

$$u/y^n = u_i/y_i^n, \tag{A 4}$$

where n is an exponent and i indicates the elevation above the mean water level. Therefore, the variation of u with vertical distance may be accounted for by dividing u by the quantity ψ^{n_1}, where

$$\psi = \left|\frac{(u_i y_i/\nu)^2}{u_i^2/g y_i}\right| = \left(\frac{Re_i}{Fr_y}\right)^2, \tag{A 5}$$

which is one of the expressions for y_i in dimensionless form; ν is the kinematic viscosity and n_1 is a constant. Thus (A 3) may be approximately expressed as

$$\frac{u_i}{(\tau_0/\rho)^{\frac{1}{2}}\psi^{n_1}} = \phi_1\left[\frac{a_{\text{r.m.s.}}}{L}, \frac{u_i}{(gL^{n_2}y_i^{1-n_2})^2}\right], \tag{A 6}$$

where n_2 is an exponent. From the experimental work discussed in § 3, the following empirical expression is obtained:

$$\frac{ku_i}{u_\tau} = 0{\cdot}7\psi^{0{\cdot}033} \ln\left[\frac{946a_{\text{r.m.s.}}/L}{(u_i/g^{0{\cdot}5}L^{0{\cdot}4}y^{0{\cdot}1})^{3{\cdot}5}}\right]. \tag{A 7}$$

Likewise, an empirical relationship between $a_{\text{r.m.s.}}/L$ and u may be deduced from the same experimental data:

$$a_{\text{r.m.s.}}/L = \exp\left[-14{\cdot}2 + 0{\cdot}08u_i(gy_i)^{-\frac{1}{2}}\psi^{0{\cdot}12}\right] \tag{A 8}$$

or

$$a_{\text{r.m.s.}}/L = 0{\cdot}008,$$

whichever is smaller. Now, combining (A 7) and (A 8) with (A 1), we have

$$\frac{1}{C_i^{\frac{1}{2}}} = -1{\cdot}23\psi^{0{\cdot}033} \ln\frac{946\exp\left|-14{\cdot}2 + 0{\cdot}08u_i(gy_i)^{-\frac{1}{2}}\psi^{0{\cdot}12}\right|}{(u_i/g^{0{\cdot}5}L^{0{\cdot}4}y_i^{0{\cdot}1})^{3{\cdot}5}}, \tag{A 9}$$

where C_i is defined by (14), as $C_i = 2(u_\tau/u_i)^2$.

Dimensionless parameters

Equations (1) and (3) can be transformed into dimensionless form using the following parameters:

$$\tilde{F} = \frac{m_{z_0} - m}{m_{z_0} - m_r} \quad \text{or} \quad \frac{t_{z_0} - t}{t_{z_0} - t_r},$$

$$u^+ = u/u_\tau, \quad v^+ = v/u_\tau, \quad x^{++} = x/z_0, \quad y^{++} = y/z_0,$$

$$\alpha + \epsilon_H = (\nu + \epsilon_M)/\epsilon_e, \quad \beta + \epsilon_D = (\nu + \epsilon_M)/\epsilon_e,$$

where the subscript r refers to a reference height above the mean water level, the subscript z_0 refers to $y = z_0$ and

$$\epsilon_e = \begin{cases} \dfrac{1 + \epsilon_M/\nu}{Pr^{-1} + Pr_t^{-1}(\epsilon_M/\nu)} & \text{for heat transfer,} \\ \dfrac{1 + \epsilon_M/\nu}{Sc^{-1} + Sc_t^{-1}(\epsilon_M/\nu)} & \text{for mass transfer.} \end{cases}$$

Here Pr is the Prandtl number ν/α, Sc is the Schmidt number ν/β and Pr_t and Sc_t are the turbulent Prandtl number ϵ_M/ϵ_H and turbulent Schmidt number ϵ_M/ϵ_D respectively.

Expressions required for transformation

In performing the transformation, the following terms have to be deduced.

(i) Eddy diffusivity for momentum. The expression for the eddy diffusivity for momentum can be deduced from the definition of the shear stress for turbulent flow. Not too far from the surface, the relationship between the shear stress at a wall and the eddy diffusivity for momentum may be expressed as

$$\tau_0/\rho = (\nu + \epsilon_M)\,\partial u/\partial y. \tag{A 10}$$

Evaluating the term $\partial u/\partial y$ from (A 1) and then substituting it into the above equation and rearranging gives

$$\nu + \epsilon_M = ku_\tau z_0 y^{++}. \tag{A 11}$$

(ii) $\partial z_0/\partial x$ and $\partial x^{++}/\partial x$. The term $\partial z_0/\partial x$ can be evaluated directly from (A 9) as

$$\partial z_0/\partial x = 0{\cdot}98\psi^{0{\cdot}033} z_0/x.$$

For $y = y_r = 153$ mm (see § 3)

$$\psi^{0{\cdot}033} = 1{\cdot}86 \quad \text{hence} \quad \partial z_0/\partial x = 1{\cdot}82 z_0/x \tag{A 12}$$

and

$$\frac{\partial x^{++}}{\partial x} = \frac{z_0 - x\,\partial z_0/\partial x}{z_0^2} = \frac{-0{\cdot}82}{z_0}. \tag{A 13}$$

(iii) $\partial u_\tau/\partial y^{++}$ and $\partial u_\tau/\partial x^{++}$. An empirical relationship between $u_\tau/(gy_r)^{\frac{1}{2}}$ and x^{++} can be obtained by fitting the experimental data of § 3. The result is

$$\ln[u_\tau/k(gy_r)^{\frac{1}{2}}] = -0{\cdot}42 \ln x^{++} + 4{\cdot}04, \tag{A 14}$$

where $x^{++} = x/z_0$. From (A 14) we have

$$\partial u_\tau/\partial z_0^{-1} = -0{\cdot}19 z_0 u_\tau. \tag{A 15}$$

Dividing the above equation by y gives

$$\partial u_\tau/\partial y^{++} = -0{\cdot}19 u_\tau/y^{++}, \tag{A 16}$$

where $y^{++} = y/z_0$. Likewise

$$\partial u_\tau/\partial x^{++} = -0{\cdot}42 u_\tau/x^{++}. \tag{A 17}$$

(iv) $\partial u^+/\partial x^{++}$. The velocity profile (A 1) can be rewritten as

$$u^+ = \frac{1}{k}\ln\frac{x}{z_0} + \frac{1}{k}\ln y - \frac{1}{k}\ln x. \tag{A 18}$$

Taking the derivative of u^+ with respect to x^{++} gives

$$\partial u^+/\partial x^{++} = 2{\cdot}23/kx^{++}. \tag{A 19}$$

REFERENCES

Braslavskii, A. P. & Vikulina, Z. A. 1963 Evaporation norms from water reservoirs. *Israel Prog. Sci. Trans. Ltd, Jerusalem* (trans. from Russian).

Calder, K. L. 1949 Eddy diffusion and evaporation in flow over aerodynamically smooth and rough surfaces: a treatment based on laboratory laws of turbulent flow with special reference to conditions in the lower atmosphere. *Quart. J. Mech. Appl. Math.* **2**, 153.

Chambers, A. J., Mangarella, P. A., Street, R. L. & Hsu, E. Y. 1970 An experimental investigation of transfer of momentum at an air–water interface. *Tech. Rep. Dept. Civil Engng, Stanford Univ.* no. 133.

Charnock, H. 1955 Wind stress on a water surface. *Quart. J. Roy. Met. Soc.* **81**, 639.

Deardorff, J. W. 1962 An experimental ocean buoy air–sea transfer studies. *Occ. Rep., Univ. Washington*, no. 13.

Fleagle, R. G., Deardorff, J. W. & Badgley, F. I. 1958 Vertical distribution of wind speed, temperature and humidity above a water surface. *J. Mar. Res.* **17**, 141.

Gottifredi, J. C. & Jameson, G. J. 1970 A growth of short waves on liquid surfaces under the action of wind. *Proc. Roy. Soc.* A **319**, 373.

Hidy, G. M. & Plate, E. J. 1966 Wind action on water standing in a laboratory channel. *J. Fluid Mech.* **26**, 651.

Kitaigorodskii, S. A. & Volkov, Yu. A. 1965 On the roughness parameter of the sea surface and the calculation of momentum flux in the near-water layer of the atmosphere. *Atmos. Ocean. Phys.* **1**, 556. (English trans. published by Am. Geophys. Un.)

MANGARELLA, P. A., CHAMBERS, A. J., STREET, R. L. & HSU, E. Y. 1972 Laboratory and field interfacial energy and mass flux and prediction equations. *J. Geophys. Res.* **77**, 5870.

MANGARELLA, P. A., CHAMBERS, A. J., STREET, R. L. & HSU, E. Y. 1973 Laboratory studies of evaporation and energy transfer through a wavy air–water interface. *J. Phys. Ocean.* **3**, 93.

MARCIANO, J. J. & HARBECK, G. E. 1954 Mass transfer studies, water loss investigations: Lake Hefner studies technical report. *Geol. Survey Prof. Paper, U.S. Dept. Interior*, no. 269.

MONIN, A. S. 1972 The atmospheric boundary layer. *Ann. Rev. Fluid Mech.* **2**, 225.

PLETCHER, R. H. 1969 On a finite-difference solution for the constant property turbulent boundary layer. *A.I.A.A. J.* **7**, 302.

PRANDTL, L. 1928 Bemerkung uber den Warneubergang im Rohr. *Phys. Z.* **29**, 325.

RUGGLES, K. W. 1970 The vertical mean wind profile over the ocean for light to moderate winds. *J. Appl. Met.* **9**, 390.

SHAW, C. Y. & LEE, Y. 1974 Turbulent transport phenomena between a large body of water and surrounding atmosphere. *Proc. 5th Int. Heat Transfer Conf., Tokyo*, vol. 4, p. 144.

SHEMDIN, O. H. 1967 Experimental and analytical investigation of the air velocity profile above progressive waves. *Tech. Rep. Dept. Civil Engng, Stanford Univ.* no. 82.

SNOPKOF, U. G. 1965 Turbulent exchange in an atmospheric layer directly above the ocean. *Trans. (Trudy) Inst. Oceanol. Acad. Sci.* no. 78.

TAKAHASHI, T. 1958 Micro-meteorological observations and studies over the sea. *Met. Notes, Kyoto Univ. Met. Res. Inst.* ser 2, no. 12.

WU, J. 1968 Laboratory studies of wind–wave interactions. *J. Fluid Mech.* **34**, 91.

WU, J. 1969 Wind stress and surface roughness at air–sea interface. *J. Geophys. Res.* **74**, 444.